Results from the Vicarious Calibration of ADEOS/AVNIR and the Visible and Near-Infrared Channels of OCTS with AVIRIS

Kohei Arai
arai@is.saga-u.ac.jp
Dept. of Information Science, Saga University
1 Honjo, Saga 840-8502 Japan

Abstract

A field campaign for the vicarious calibration of the instruments ADEOS/AVNIR (Advanced Earth Observing Satellite/Advanced Visible and Near-Infrared Radiometer) and the visible to near-infrared channels of the Ocean Color and Temperature Scanner (OCTS) was conducted based on the reflectance-based method. The results show a not so small difference between the estimated top of atmosphere (ToA) radiance and the instruments' data-derived radiance, i.e., 3.5 to 20%. In order to confirm the validity of the difference, vicarious calibration based on the radiance-based method was conducted using Airborne Visible/Infrared Imaging Spectrometer (AVIRIS) data. Also, an effect due to the spectral refractive index of aerosol on the estimation of the ToA radiance was confirmed, together with smear-like image defect in the AVNIR imagery data.

1. Introduction

There are two well-defined methods for vicarious calibration of spectral radiometers onboard satellites: (1) reflectance-based and (2) radiance-based [1–4]. The Advanced Earth Observing Satellite/Advanced Visible and Near-Infrared Radiometer (ADEOS/AVNIR) and the visible to near-infrared channels of Ocean Color and Temperature Scanner (OCTS) were calibrated using the reflectance-based method [5–7]. The results show a significant discrepancy—5 to 12%—between the estimated top of atmosphere (ToA) radiance and the instruments' data-derived radiance [8]. From an error budget analysis, it is clear that the vicarious calibration accuracy of the radiance-based method is better than that of the reflectance-based method, in general, if well-calibrated airborne instrument spectral radiometer data is acquired simultaneously with satellite data as well as ground-based measurements. In order to confirm the significant discrepancy, ADEOS/AVNIR and the visible to near-infrared channels of OCTS were re-calibrated using the radiance-based method with well-calibrated AVIRIS data, which was provided by the U. S. National Aeronautics and Space Administration/Jet Propulsion Laboratory (NASA/JPL) through Japan's National Space Development Agency (NASDA) under a contract between NASA and NASDA.

There are many factors influencing vicarious calibration accuracy. It is not so difficult to accurately estimate molecule optical depth (Rayleigh Scattering), optical depth of ozone, and water vapor compared to that for aerosol optical depth (Mie Scattering). One of the largest error sources is estimation of the refractive index of aerosol, which depends on aerosol type and size distribution of aerosol particles, and vertical profile in the atmosphere. Moreover, the refractive index of aerosol has spectral characteristics, so it is better to take into account the spectral refractive index in the estimation of aerosol optical depth.

First, the results from the vicarious calibration of ADEOS/AVNIR and the visible to near-infrared channels of OCTS is briefly described, followed by the results from the radiance-based vicarious calibration. Then the influence due to the spectral refractive index is followed together with the other error sources, in particular, bidirectional reflectance distribution function (BRDF) effect. Also, a smear-like image defect observed in the ADEOS/AVNIR is described.

2. A Brief Description of Previous Vicarious Calibration Results Based on the Reflectance-Based Method

2.1 Major Characteristics of ADEOS/AVNIR and OCTS

The wavelength coverage of ADEOS/AVNIR and the visible and near-infrared channels of OCTS are shown in Table 1.

Table 1. Major Characteristics of ADEOS/AVNIR and the Visible to Near Infrared Channels of OCTS

Center Wave-length	AVNIR	460 (Mu1)	560 (Mu2)	650 (Mu3)	825 (Mu4)	605 (Pa)			
	OCTS	412	443	490	516	565	667	765	862
Band-Width	AVNIR	80	80	80	130	170			
	OCTS	18	20	23	15	19	21	41	39

Mux: Multi-spectral band x, Pa: Panchromatic band

AVNIR is 18 m of spatial resolution of multi-spectral visible to near-infrared radiometer while OCTS is 800 m of spatial resolution of ocean color and temperature scanner.

2.2 Field Campaign

The field campaign was conducted at Ivanpah Playa, California, situated on the border with Nevada, on March 4, 1997. The conditions of the field campaign are shown in Table 2.

Table 2. The Conditions for the Field Campaign for Vicarious Calibration of ADEOS/AVNIR and the Visible to Near-Infrared Channels of OCTS

Date	Location	Lat/Lon	Sunrise	Overpass	Solar Noon
1997/3/4	Ivanpah Playa	35N/115W	6:07	10:49:59	11:52
Surface Pressure	Humidity	Air Temperature	Solar Azimuth	Solar Zenith	Pointing Angle
930 (hPa)	48 (%)	284 (K)	156.8 (deg)	45.0 (deg)	3.6 (deg)

Two days before the field campaign, it rained, so the surface of the test site was dry and the reflectance high. The atmosphere was so clear that curve fitting results between the measured optical depth (368-, 500-, 675-, 778-, 862-nm channels of sun-photometer were used), and the MODTRAN 4.0 derived optical depth shows that the meteorological range is better than 50 km. The sun-photometer used was well calibrated through Langley plots in clear sky conditions, in particular, at the top of the Mauna Loa mountain in Hawaii. Meanwhile, the spectral radiometer used for surface reflectance measurements was also well calibrated, with higher than 1% stability of the gain for short-term measurements (more than 1 hour). The radiometer covers from 500 nm to 999 nm for the visible to near-infrared, with 10 nm of spectral resolution and 1300 nm to 2599 nm for the short-wave infrared region, with 20 nm of spectral resolution. On the other hand, Spectralon® was used for the reference plaque. In the calculation of surface reflectance, the BRDF of the Spectralon was taken into account [9].

2.3 Comparisons of ToA Radiance from the ADEOS/AVNIR- and OCTS-Derived Data and the Field Campaign Data

The results from the field campaign are shown in Tables 3 and 4.

Table 3. A Comparison Between Estimated with Field Campaign Data and Derived from ADEOS/AVNIR Data

Band	Estimated ToA	Digital Number Derived ToA	% Difference
1	89.46	86.33	-3.5
2	140.40	130.29	-7.2
3	112.90	90.09	-20.2
4	93.82	75.43	-19.6

Table 4. A Comparison Between Estimated with Field Campaign Data and Derived from ADEOS/OCTS Data

Band	Estimated ToA	Digital Number Derived ToA	% Difference
1	87.60	75.84	-15.5
2	95.73	86.09	-11.2
3	102.54	93.05	-10.2
4	94.36	86.25	-9.4

3. Vicarious Calibration Using the Radiance-Based Method

3.1 AVIRIS Data Used

Figure 1 shows the AVIRIS-derived AVNIR and the real AVNIR data. The instantaneous field of view (IFOV) and spectral response are adjusted to the AVNIR. A smear-like image defect is seen in all the bands of the real AVNIR images.

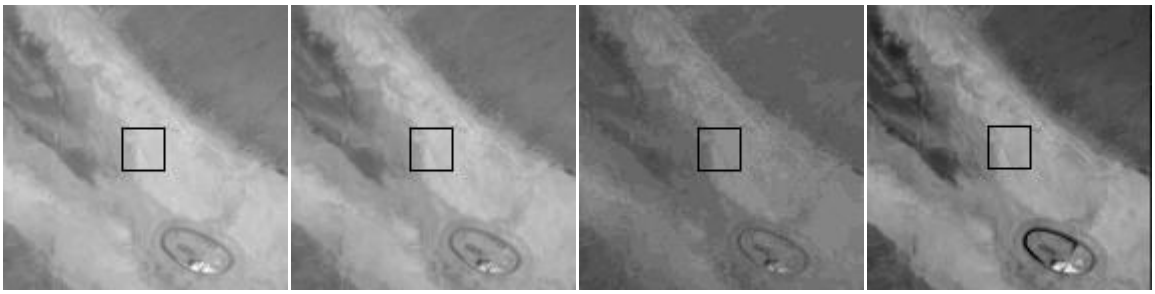

(1) AVIRIS-AVNIR 1 (2) AVIRIS-AAVNIR 2 (3) AVIRIS-AVNIR 3 (4) AVIRIS-AVNIR 4

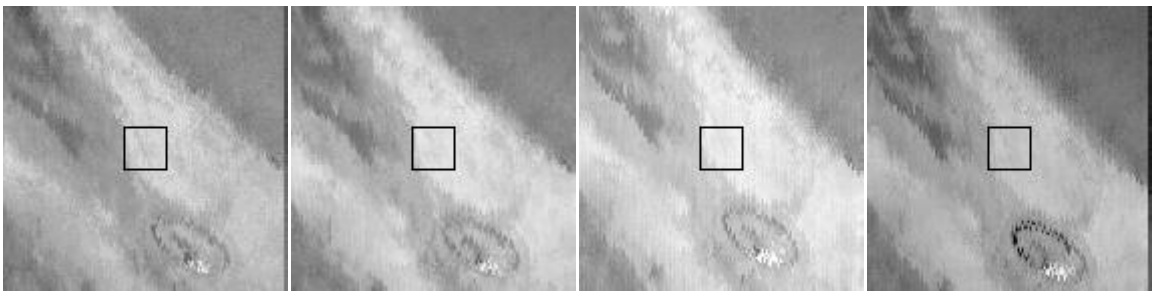

(5) Real AVNIR 1 (6) Real AVNIR 2 (7) Real AVNIR 3 (8) Real AVNIR 4

Figure 1. The AVIRIS-Derived AVNIR and the Real AVNIR Data (Bands 1 to 4, From the Top to the Bottom) of Ivanpah Playa, California, on March 4, 1997.

3.2 Estimation of ToA Radiance Using the Radiance-Based Method

There are many factors influencing vicarious calibration accuracy. It is not so difficult to accurately estimate molecule optical depth (Rayleigh Scattering), optical depth of ozone, and water vapor compared to that for aerosol optical depth (Mie Scattering). One of the largest error sources is estimation of the refractive index of aerosol, which depends on aerosol type and size distribution of aerosol particles,

vertical profile in the atmosphere. Moreover, the refractive index of aerosol has spectral characteristics, so it is better to taken into account the spectral refractive index in the estimation of aerosol optical depth.

From Total Ozone Mapping Spectrometer (TOMS) data, the total ozone (column) was estimated. By using spectral absorption coefficients provided by World Meteorological Organization (WMO), optical depth due to ozone was estimated. Also, optical depth due to water vapor was estimated, with relative humidity measured at the surface. By using MODTRAN 4.0, a vertical profile of the water vapor was estimated, based on a scaling with the relative humidity on the ground, in accordance with the Mid-Latitude Summer model of MODRAN 4.0.

Using an empirical model of the aerosol, the refractive index of the test site, Ivanpah Playa, in this season was assumed to be 1.44-i0.005, while 3.622 of the Junge parameter was estimated from the optical depth measurement. Then, a ToA radiance was estimated using the Gauss-Seidel Model based atmospheric code (plane parallel atmosphere) as a radiative transfer model, taking multiple scattering in the atmosphere into account.

3.3 Spectral Characteristics of the Refractive Index

Meanwhile, the refractive index has spectral characteristics. The value 1.44-i0.005 implies mixed aerosol particles between water soluble and oceanic aerosols, with the mixing ratio of 0.5 and 0.5, respectively, based on Maxwell-Garnet Mixing Model. Figures 2 and 3 show the characteristics of the real and the imaginary parts of the refractive index for five typical aerosol types: soot, oceanic, water soluble, dust and 75% H_2SO_4. As is shown in the figure, the imaginary part of the water-soluble aerosol has enough of this spectral characteristic to be taken into account. Figure 4 shows the real and imaginary parts of the refractive index of 50 by 50 of oceanic and water soluble.

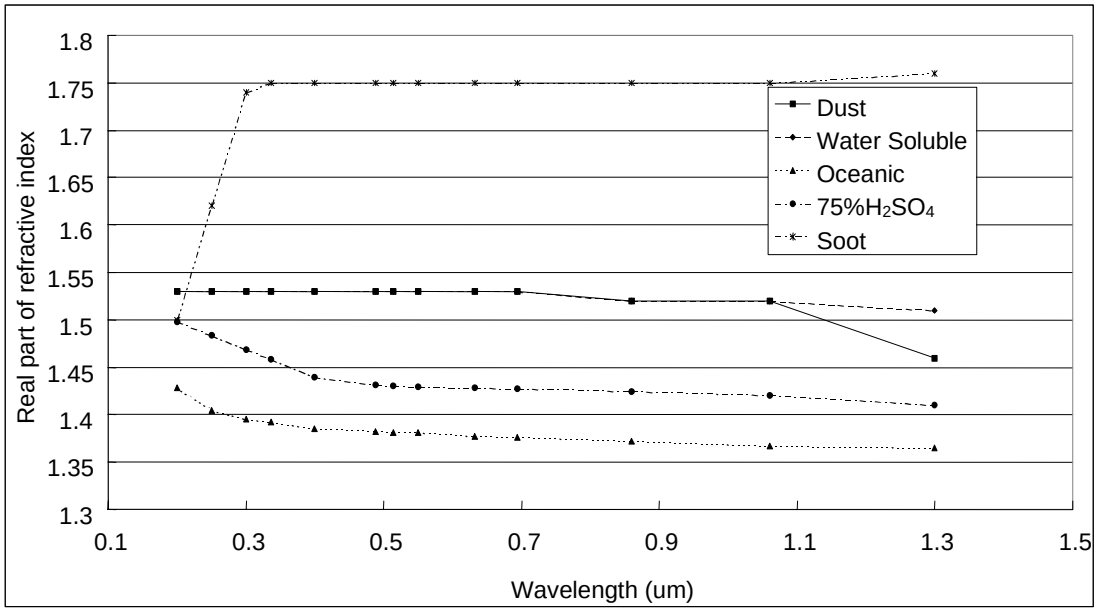

Figure 2. Spectral Characteristics of the Real Part of the Refractive Index.

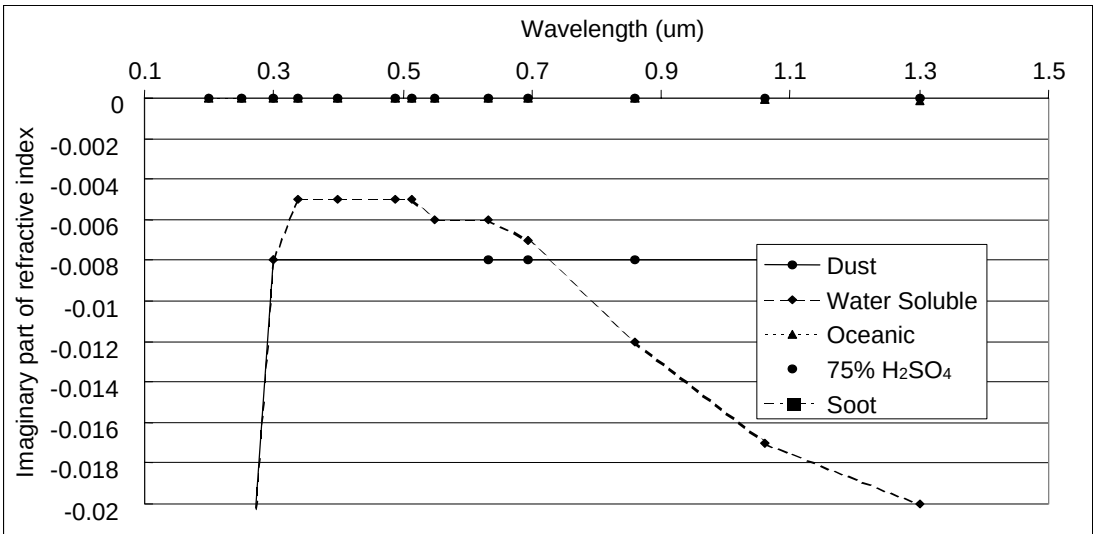

Figure 3. Spectral Characteristics of the Imaginary Part of the Refractive Index.

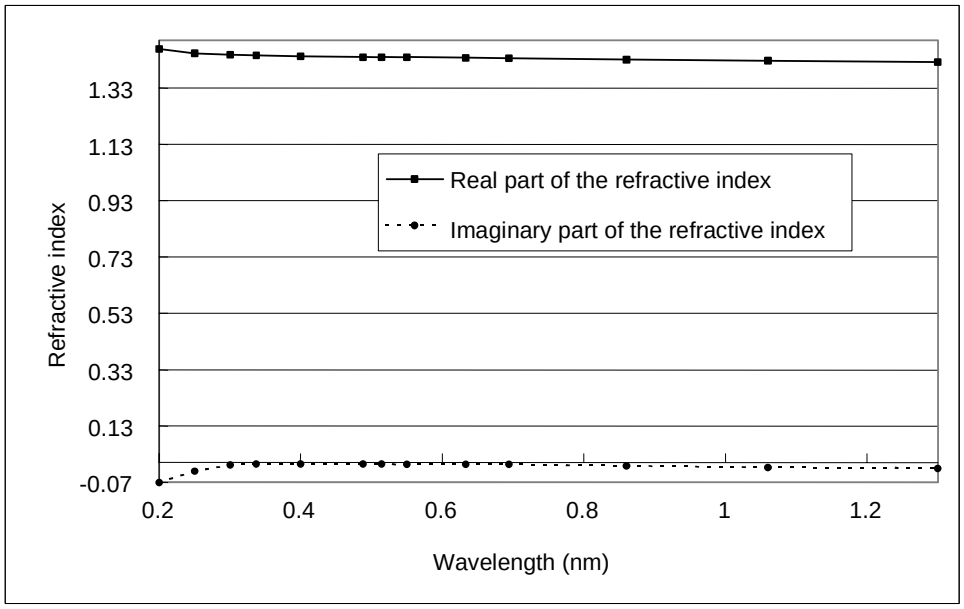

Figure 4. The Refractive Index of 50 by 50 of Mixed Aerosol Between Oceanic and Water Soluble Aerosols.

At the center of the square is the location of test site. In the square, the reflectance in the 36 x 36 m of area was measured. From the estimated parameters with the measured optical depth, atmospheric pressure, relative humidity, TOMS derived column ozone in unit of Dobson unit (DU) and assumed refractive index and size distribution as well as meteorological range from the curve fitting with MODTRAN 4.0, ToA radiance was estimated together with the up-welling radiance at the altitude of 20 km (AVIRIS altitude) based on MODTRAN 4.0. Table 5 shows the single scattering albedo (Omega), path radiance (PathRad.), up-welling radiance of direct component (Direct) and gaseous transmittance (Gaseous) for the ToA radiance under the assumption of the Junge parameter of 3.0 and refractive index of 1.44-i0.005 (first part of the table), for the up-welling radiance at the altitude of 20 km (AVIRIS altitude) (second part of the table), for the ToA radiance taking into account the spectral characteristics of the refractive index (third part of the table) and for the up-welling radiance at the altitude of 20 km (AVIRIS altitude) (bottom part of the table).

3.4 Comparison of ToA Radiance

Results from the comparison of the estimated radiance with and without consideration of the spectral characteristics of the refractive index of aerosol are shown in Figures 5 and 6. In accordance with the change of the transparency above 20-km atmosphere, which is shown in Figure 5, the path radiance, in particular, affects ToA radiance. In the radiance-based method, the difference between actual AVIRIS-derived AVNIR radiance and the estimated up-welling radiance with MODTRAN 4.0 is adjusted in the ToA radiance calculation.

Table 5. The single scattering albedo (Omega), path radiance (PathRad.), up-welling radiance of direct component (Direct) and gaseous transmittance (Gaseous)

ToA	3 1.44-0.005i				
AVNIR Band	ToA	Omega	PathRad.	Direct	Gaseous
1	89.46	0.943681	33.10494	47.15204	0.897127
2	140.4	0.943162	35.47947	104.8832	0.999734
3	112.9	0.942481	10.3049	94.8752	0.931622
4	93.82	0.938002	4.891018	84.38399	0.951556
20-km	3 1.44-0.005i				
AVNIR Band	20-km	Omega	PathRad.	Direct	Gaseous
1	88.43348	0.943681	31.38323	47.73283	0.894639
2	142.7767	0.943162	22.23247	107.7011	0.910047
3	114.3207	0.942481	9.929993	96.52892	0.93123
4	93.84546	0.938002	4.660277	84.62563	0.951414

ToA	3 Spectral				
AVNIR Band	ToA	Omega	PathRad.	Direct	Gaseous
1	89.46214	0.943787	33.10765	47.15204	0.897136
2	140.2458	0.943787	35.34943	104.8832	0.999906
3	112.7916	0.930559	10.24988	94.8752	0.932029
4	93.36738	0.859744	4.680581	84.38396	0.953915
20-km	3 Spectral				
AVNIR Band	20-km	Omega	PathRad.	Direct	Gaseous
1	88.43537	0.943787	31.3858	47.73283	0.894649
2	142.6199	0.943787	22.15099	107.7013	0.910478
3	114.2112	0.930559	9.876302	96.52892	0.931653
4	93.39988	0.859744	4.457769	84.62563	0.953785

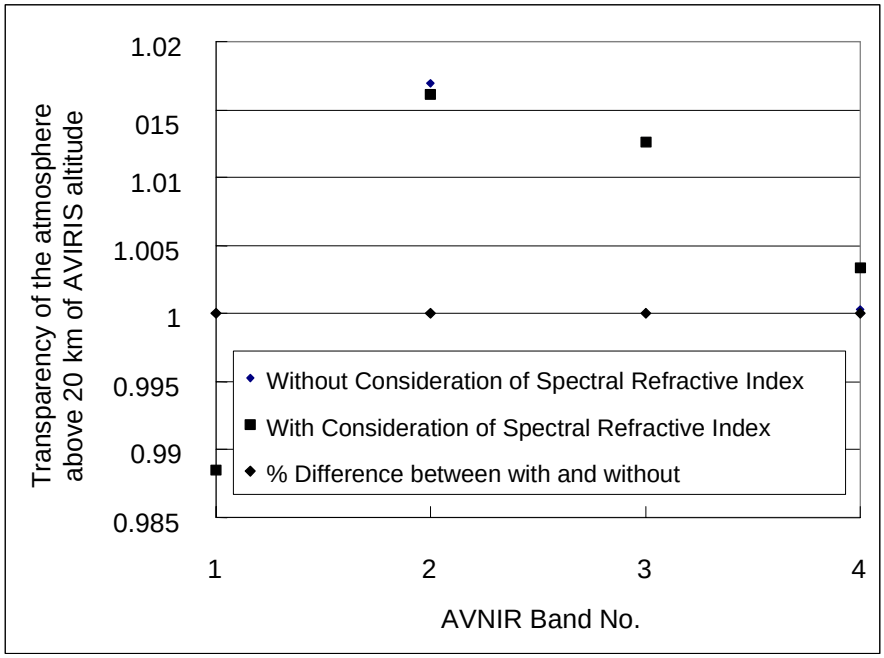

Figure 5. Transparency of the atmosphere from the 20 km altitude (AVIRIS altitude) to the top of the atmosphere.

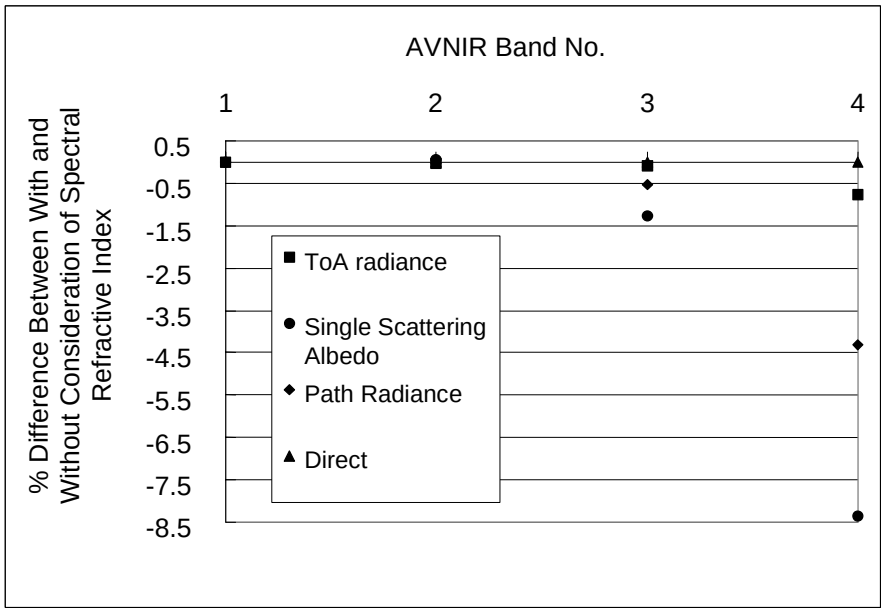

Figure 6. Percent Difference of ToA Radiance With and Without Consideration of Spectral Characteristics of the Refractive Index of Aerosol.

4. Concluding Remarks

It was found that the influence due to the spectral refractive index to ToA radiance was around 0.5% in maximum (AVNIR Band 4). It was also found that the difference between the estimated ToA and AVNIR DN-derived radiance was still large—3 to 18%—even when the radiance-based method was employed. The AVIRIS-derived AVNIR radiance and the estimated ToA radiance showed a good coincidence so that it may concluded that AVIRIS provides a qualified radiance. Moreover, smear-like image defect observed in the real AVNIR imagery data is significant.

Acknowledgements

The author would like to thank Dr. Stuart Biggar and Kutis Thome of the University of Arizona for their valuable discussions. The AVIRIS data used is provided by NASA/JPL through NASDA so that the author would also like to express his deep thanks to Dr. R. Green of NASA/JPL and Dr. S. Shimada of NASDA/EORC (Earth Observation Research Center).

References

[1] P. Slater, S. Biggar, R. Holm, R. Jackson, Y. Mao, M. Moran, J. Palmer and B. Yuan, Reflectance and radiance based methods for the in-flight absolute calibration of multispectral sensors, Remote Sensing of Environment, 22, 11-37, 1987.

[2] K. Arai, Fundamental Theory for Remote Sensing, Gakujutsu Tosho Shuppan Pub.Co., Ltd., 144, 2001.

[3] K. Arai and K. Thome, Error Budget Analysis of Vicarious Calibration Based on Reflectance Based Method, Journal of Japan Society of Photogrammetry and Remote Sensing, 39, 2, 74-81, 2000.

[4] K. Arai, K. Thome, S. Tsuchida, T. Takashima, S. Machida and H. Tonooka, A Field Experiment at Tsukuba Test Site for Vicarious Calibration of ASTER (Visible to Shortwave Infrared Wavelength Region), Journal of Remote Sensing Society of Japan, 20, 1, 55-62, 2000.

[5] K. Arai and Y. Terayama, An Experimental Approach for Vicarious Calibration of ADEOS/AVNIR and the Visible Channels of OCTS, Journal of Japan Society of Photogrammetry and Remote Sensing, 38, 6, 34-40, 2000.

[6] K. Arai, N. Ebuchi, G. Jaross and M. Moriyama, The Results from the Cross Calibration and Validation of the Instruments Onboard ADEOS Satellite, Journal of Remote Sensing Society of Japan, 17, 5, 19-25, 1997.

[7] M. Naka, I. Sato, S. Tsuchida, Y. Kawata, A. Yamazaki, M. Imanaka and K. Arai, An Interim Report on CAL/VAL Study for the ADEOS/AVNIR, Journal of Remote Sensing Society of Japan, 17, 5, 32-40, 1997.

[8] K. Thome, S. Shiller, J. Cornel, K. Arai and S. Tsuchida, Results of the 1996 EOS vicarious calibration joint field campaign at Lunar Lake Playa, Nevada (USA), Metrologia, 35, 631-638, 1999.

[9] K. Thome, F. Palluconi, K. Arai, S. Hook, H. Tonooka and S. Tsuchida, Inflight Radiometric Calibration of ASTER, American Geophysics Union, Spring, Boston, May, 2001.